

*Full Length Research Paper*

# Simulation of the wire reverse bending test

Kazeem K. Adewole\* and Steve J. Bull

Chemical Engineering and Advanced Materials, Newcastle University, Newcastle upon Tyne,  
United Kingdom, NE1 7RU.

Accepted 29 February, 2012

Steel wires are used for pre-stressing concrete structural units and for the construction of suspension bridges among other applications in civil engineering. The reverse bending and straightening of wires by rollers is employed as a routine quality check to detect laminations in wires. Experimental work on the reverse bending of wires and Finite Element (FE) simulation of bending of wires has been investigated previously but the simulation of the reverse bending and straightening of wire has not been studied in detail. Also, the FE simulation of the bending of wire round a mandrel reported in the literature was conducted by pinning the nodes on one end of the wire to the mandrel and applying a concentrated load to the free end of the wire to bend the wire, which does not replicate the bending process in practice. In this paper, three dimensional FE simulation of the reverse bending of steel wires conducted as a part of the research to investigate the effects of the combination of reverse bending and defects such as laminations and scratches on the wires is presented. It is demonstrated that the reverse bending simulation procedures employed are appropriate based on a good agreement with experimental results.

**Key words:** Steel wires, finite element (FE) simulation, reverse bending, lamination.

## INTRODUCTION

Steel wires are used for pre-stressing concrete structural units such as beams and girders, and for the construction of suspension bridges among other applications in civil engineering. The reverse bending and straightening of wires is employed as a quality check to detect laminations in wires. A lamination is a material separation or discontinuity, which is normally invisible at the surface and is generally parallel to the rolling or drawing direction (Smith et al., 1957). Laminations result from defects such as cylindrical cavities in the parent ingot, slag or mould powder entrapment in the casting process, non-metallic inclusions or alloy segregation that are elongated in the rolling or drawing direction during material working (Smith et al., 1957; Moir and Preston, 2002; Escoe, 2006; Peet and Wilde, 2001). Crack-like laminations (longitudinal cracks) have been found to be instrumental to the fractures of the pre-stressing wire of ruptured pre-

stressed concrete pipe (United States Bureau of Reclamation, 1994). Figure 1 shows the typical arrangement of three rotating rollers used for the routine reverse bending and straightening of flat wires. Typically, the rollers are 100 mm in diameter and the wires are bent over the left hand roller, reverse bent over the middle roller and finally straightened over the right hand roller.

Most of the published literature on bending and reverse bending of metal products such as the work of Firat (2007), Gau and Kinzel, (2001), Ken-ichiro (2001) and Carbonnie et al. (2008) among others, relates to the processing of sheet metal during sheet metal forming operations. The literature that specifically deals with the bending and reverse bending of wires includes the experimental work conducted by Gillstrom and Jarl (2006) on reverse bending for descaling of wire rods and the experimental and Finite Element (FE) simulation works conducted by Burks et al. (2009, 2010) on the effect of excessive bending on the axial compressive stress and the residual tensile strength of aluminium conductor composite core (ACCC) wires.

Burks et al. (2009, 2010) conducted a FE simulation of

\*Corresponding author. E-mail: [kkadewole@yahoo.com](mailto:kkadewole@yahoo.com). Tel: +2348092540024.

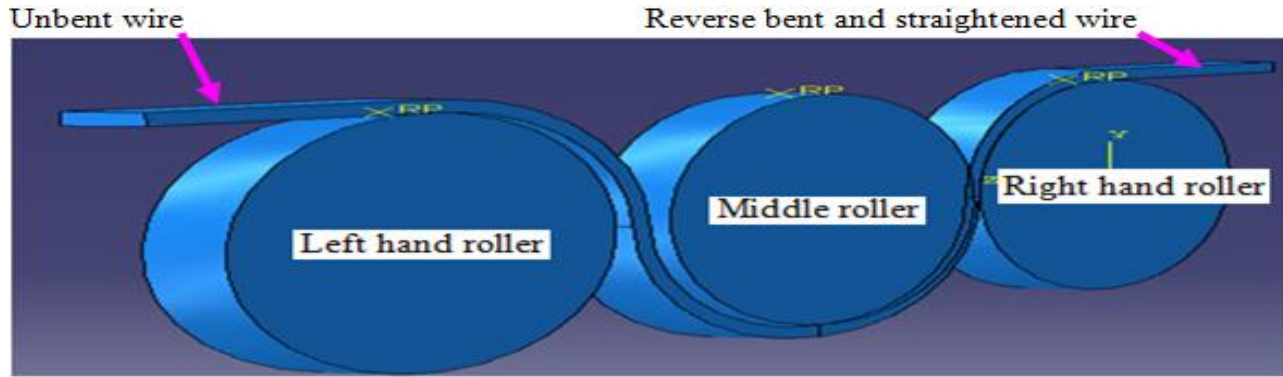


Figure 1. Industrial reverse bending equipment with three rollers.

the bending of the ACCC wire round a mandrel by pinning the nodes on the end of the ACCC rod that are in contact with the mandrel at the beginning of the simulation and applied a concentrated load to the free end of the wire to bend the rod round the mandrel. Although this methodology may produce the desired bending effects in the wire, it does not replicate the bending process in practice. In practice, the mandrel is rotated and the wire is bent and wrapped round the rotating mandrel. Also, this modelling approach of bending the wire round the static mandrel instead of the rotating mandrel bending the wire round it could not be used to simulate the reverse bending of wires over the second roller without having to unwind the bent wire from the first roller, thereby introducing the unwinding process which is not part of the reverse bending process in practice.

For a wire of diameter,  $\phi$ , or thickness,  $T$ , bent over a roller with diameter,  $D_r$ , elongation,  $e$ , occurs at the top or outer surface of a wire while compression occurs at the interface between the rod and the roller leading to stretching of the outer fibre and the compression of the inner fibre of the wire (Gillstrom and Jarl, 2006). The maximum elongation which occurs at the top surface of the wire can be calculated by the expression in Equation 1 obtained from Gillstrom and Jarl (2006).

$$e = \frac{T}{T + D_r} \tag{1}$$

In this paper, three-dimensional FE simulation of the reverse bending and straightening of steel wires was conducted as a part of the research to investigate the effects of the combination of reverse bending and defects such as laminations and scratches on the tensile properties of wires. The reverse bent and straightened (RBS) specimen and the unbent wire specimen were subjected to a tensile testing simulation to determine the effect of the reverse bending and straightening process

on the wire in terms of the force-displacement response. The force-displacement curves from the FE simulation of the tensile testing of the RBS and unbent wire specimens were then validated with the force-displacement curves from the laboratory tensile testing of unbent and experimentally RBS wire specimens. The FE simulation was conducted using the combined hardening plasticity models combined with the phenomenological shear damage failure model in-built in the Abaqus v 6.9.3 material library which has been identified by Adewole et al. (2011) as an appropriate fracture model for the wire considered in this work. The details of these models are further discussed. The flat wire considered in this work is a typical high strength carbon steel wire used to provide tensile reinforcement for flexible pipes and other engineering structures.

### Combined hardening plasticity model

The combined hardening plasticity model used for this simulation is a combination of the nonlinear kinematic and isotropic hardening models. The isotropic cyclic hardening component is based on the exponential law given in Equation 2 obtained from Simulia (2007). The kinematic hardening component is based on the evolution of the backstress (a nonlinear evolution of the centre of the yield surface)  $\dot{\alpha}$  given in Equation 3 obtained from Simulia (2007).

$$\sigma^0 = Y_i + Q_\infty (1 - e^{-b\varepsilon^{pl}}) \tag{2}$$

$$\dot{\alpha} = C \frac{1}{\sigma_0} (\sigma - \alpha)^{-pl} - \gamma \alpha^{-pl} \tag{3}$$

Here,  $\sigma^0$  is the magnitude of the yield surface (the limit of the elastic range),  $Y_i$  is the initial yield stress,  $Q_\infty$  is the maximum stress increase in the elastic range,  $\varepsilon^{pl}$  is the



**Figure 2.** Experimental simulation of reverse bending of tensile armour wire.

plastic strain, and  $b$  is a material parameter that defines the rate at which the maximum is reached as plastic straining develops.  $\alpha$  is the overall backstress,  $C$  and  $\gamma$  are kinematic hardening parameters, which are material parameters that define the initial hardening modulus and the rate at which the hardening modulus decreases with increasing plastic strain, respectively (Simulia, 2007).

### Shear failure model

The shear failure criterion is a phenomenological model for predicting the onset of damage due to shear bands. Applied stress causes shear band formation and localisation, leading to the formation of cracks within the shear bands and eventual failure (Simulia, 2007). The shear model assumes that the equivalent plastic strain at the onset of damage  $\bar{\varepsilon}_s^{pl}$  is a function of the shear stress ratio  $\theta_s$  and equivalent strain rate  $\dot{\varepsilon}^{pl}$ . The shear stress ratio is calculated using the expression in Equation 4 obtained from (Simulia, 2007).

$$\theta_s = (q + k_s p) / \tau_{\max} \quad (4)$$

Where  $\tau_{\max}$ , Maximum shear stress;  $k_s$ , material parameter.

The criterion for shear damage initiation is met when the condition in Equation 5 is satisfied:

$$\omega_s = \int \frac{d\bar{\varepsilon}^{pl}}{\bar{\varepsilon}_s^{pl}(\theta_s, \dot{\varepsilon}^{pl})} = 1 \quad (5)$$

$\omega_s$  is a state variable that increases monotonically with

plastic deformation proportional to the incremental change in equivalent plastic strain. At each increment during the analysis the incremental increase in  $\omega_s$  is calculated using the expression in Equation 6 obtained from Simulia (2007).

$$\Delta\omega_s = \frac{\Delta\bar{\varepsilon}^{pl}}{\bar{\varepsilon}_s^{pl}(\theta_s, \dot{\varepsilon}^{pl})} \geq 0 \quad (6)$$

### EXPERIMENTAL AND FE ANALYSIS PROCEDURES

The details of the experimental and FE simulations are presented here.

#### Laboratory reverses bending, straightening and tensile testing of wires

The reverse bending, straightening and tensile testing of RBS wire specimen was simulated experimentally in the laboratory by winding a length of the flat wire with  $12 \times 5$  mm cross-sectional dimension round a 100 mm roller as shown in Figure 2. The bent wire length was then reverse bent in the opposite direction over the same 100 mm roller. The reverse bent wire length was finally straightened and cut into tensile test specimens. The RBS specimen and the unbent specimen were then subjected to tensile testing using an Instron universal testing machine (I  $\times$  4505) fitted with an Instron 2518 series load cell with a maximum static capacity of  $\pm 100$  kN. The displacement was measured using an Instron 2630-112 clip-on strain gauge extensometer with a 50 mm gauge length.

#### Reverse bending and straightening simulation procedures

The FE simulation of the bending, reverse bending, straightening and tensile testing of the flat wire was conducted in four simulation steps. Figure 3 shows the arrangement used for the simulation which consists of a 305 mm long tensile armour wire strip between the left roller (Roller 1) and the right roller (Roller 2) and a guide plate. The guide plate was introduced to prevent Roller 2 from lifting vertically upward during the bending simulation. The 305 mm long wire consist of a 50 mm long central tensile testing specimen and two 127.5 mm long left and right attachments. The attachments were introduced to prevent localised deformation of the ends of the tensile testing specimen, which occurred when the specimen was bonded to the rollers directly. The whole model was meshed with C3D8R elements (8-node hexahedral linear brick reduced integration elements with hourglass control). The rollers and the guide plate were meshed with  $3 \times 3 \times 3$  mm elements while the attachments and the specimen were meshed with elements having  $3 \times 3 \times 0.5$  mm and  $3 \times 1 \times 0.5$  mm dimensions, respectively. The 1 mm dimension is along the specimen length and the 0.5 mm dimension is along the specimen thickness, which translates to 10 elements along the wire thickness. The specimen was meshed with the finest mesh in order to obtain accurate results as the tensile testing simulation was carried out on the 50 mm long specimen alone. The rollers, the guide plate and the attachments (which were only introduced to prevent localised deformation of the ends of the specimen) were meshed with a coarse mesh to reduce the output file size and computation time.

The bending simulation was conducted by rotating Roller 1 in an anticlockwise direction to wind the wire round Roller 1. The reverse bending simulation was conducted by rotating Roller 1 in a

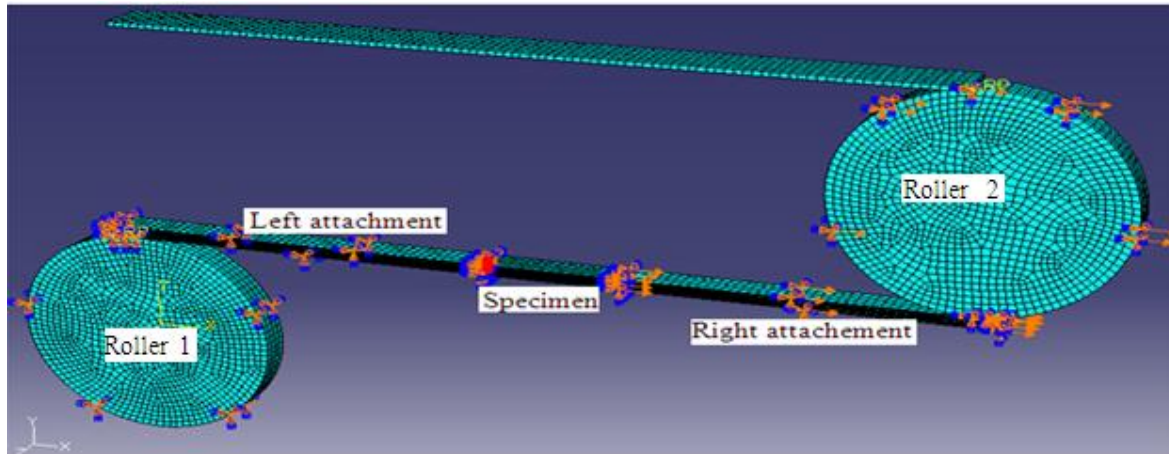


**Figure 3.** Assembly of specimen, attachments, rollers and guide plate showing the boundary condition during tensile testing simulation.

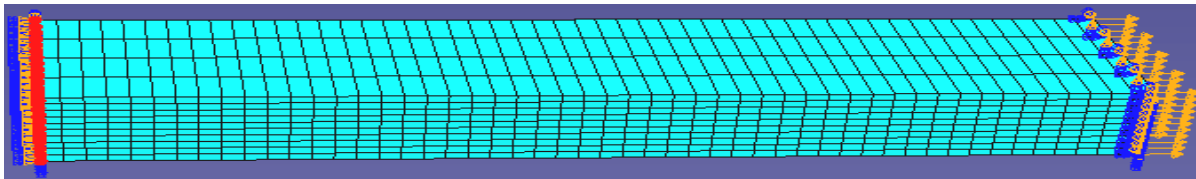


**Figure 4.** Boundary condition during the simulation of the tensile testing simulation of the unbent wire specimen.

clockwise direction to unwind the wire whilst simultaneously rotating Roller 2 in an anticlockwise direction to reverse bend and wind the wire round Roller 2. The straightening simulation was conducted by rotating Roller 2 in a clockwise direction to unwind the tensile armour wire and pulling Roller 1 longitudinally and vertically simultaneously, until the attachments and test specimen were straightened.

#### Tensile testing simulation procedures

The simulation of the tensile testing of the RBS wire specimen model was conducted on the model of the wire specimen within the rollers-attachments-specimen assembly. In order to establish the appropriate boundary conditions to be used for the simulation of the tensile testing of the RBS wire specimen within the rollers-attachments-specimen assembly, tensile testing simulations were conducted on the model of an unbent wire within the rollers-attachments-specimen assembly. The left hand end of the specimen, the left roller and the left attachment were fixed, while the right hand end of the specimen, the right roller and the right attachment, which were free to move only in the tensile load direction were subjected to a longitudinal axial tensile displacement in the tensile load direction. The results in terms of the force-displacement response and the fractured shape were then compared with the result of the tensile testing simulation conducted on an unbent wire specimen alone. The left hand end of the specimen alone was fixed, while the right hand end of the specimen alone, which was free to move only in the tensile load direction, was subjected to a longitudinal axial tensile displacement in the tensile load direction as shown in Figure 4. A good agreement between the results of the tensile testing simulation

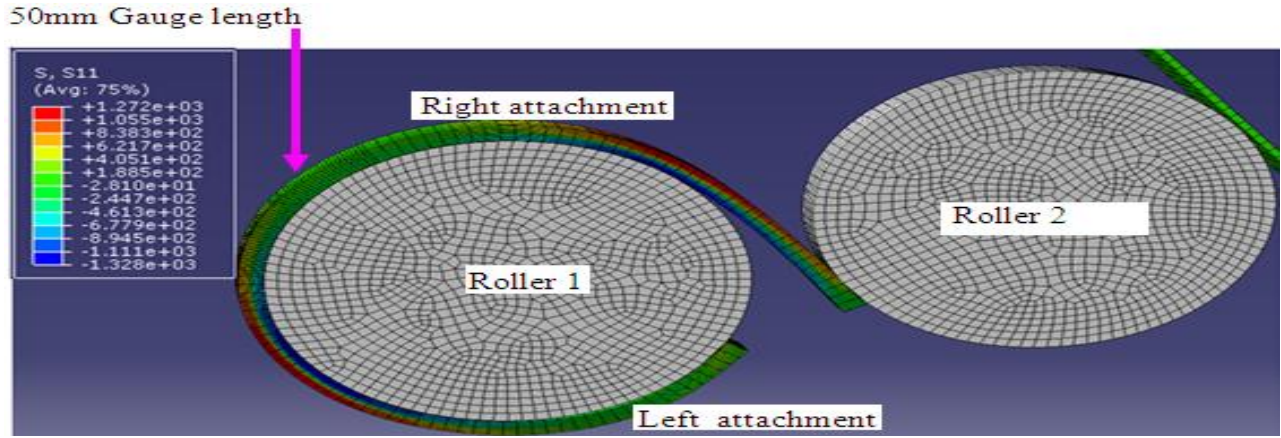
conducted with the unbent wire specimen within the rollers-attachments-specimen assembly and the unbent wire specimen alone was then established as further presented. The same simulation boundary conditions applied to the tensile testing of the unbent wire specimen within the rollers-attachments-specimen assembly was then applied to the tensile testing simulation of the RBS wire specimens within the rollers-attachments-specimen assembly.

## RESULTS

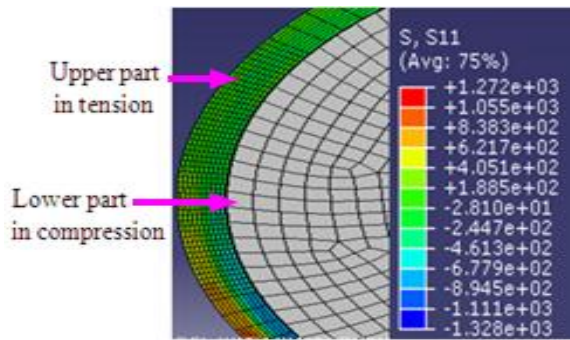
The results in terms of the deformed shapes showing the stress and strain distributions at the various stages of the bending, reverse bending, straightening and tensile testing process simulations are presented here. All the force-displacement curves in this paper are normalised with experimental ultimate load and displacement at fracture.

#### Bending, reverse bending and straightening simulation results

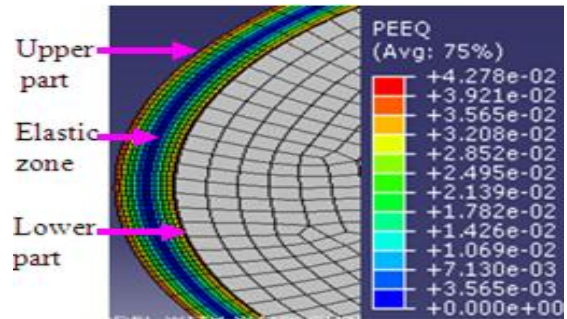
The deformed shape of the entire 305 mm long wire strip showing the longitudinal axial stress (designated as S11 in the contour plot) distribution in the wire and the position of the 50 mm gauge length tensile test specimen after the



a



b



c

**Figure 5.** Deformed shape showing longitudinal axial stress (MPa) and equivalent plastic strain distributions in wire after bending process simulation. a, Deformed shape showing longitudinal axial stress distribution; b, specimen longitudinal axial stress distribution; c, equivalent plastic strain.

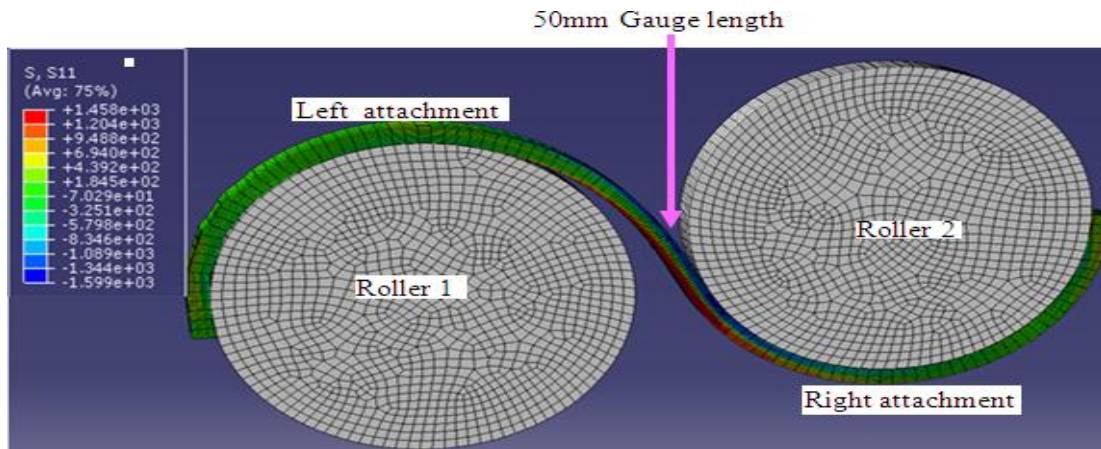


**Figure 6.** Deformed shape showing longitudinal axial stress (MPa) distribution in specimen during reverse bending process simulation.

bending simulation, during the reverse bending simulation, after the reverse bending simulation and after the straightening process simulations are shown in Figures 5a, 6, 7a and 8a, respectively. The through

thickness longitudinal axial stress distribution in the tensile test specimen after the bending, reverse bending and straightening processes simulations are shown in Figures 5(b), 7b and 8b, respectively. Positive axial

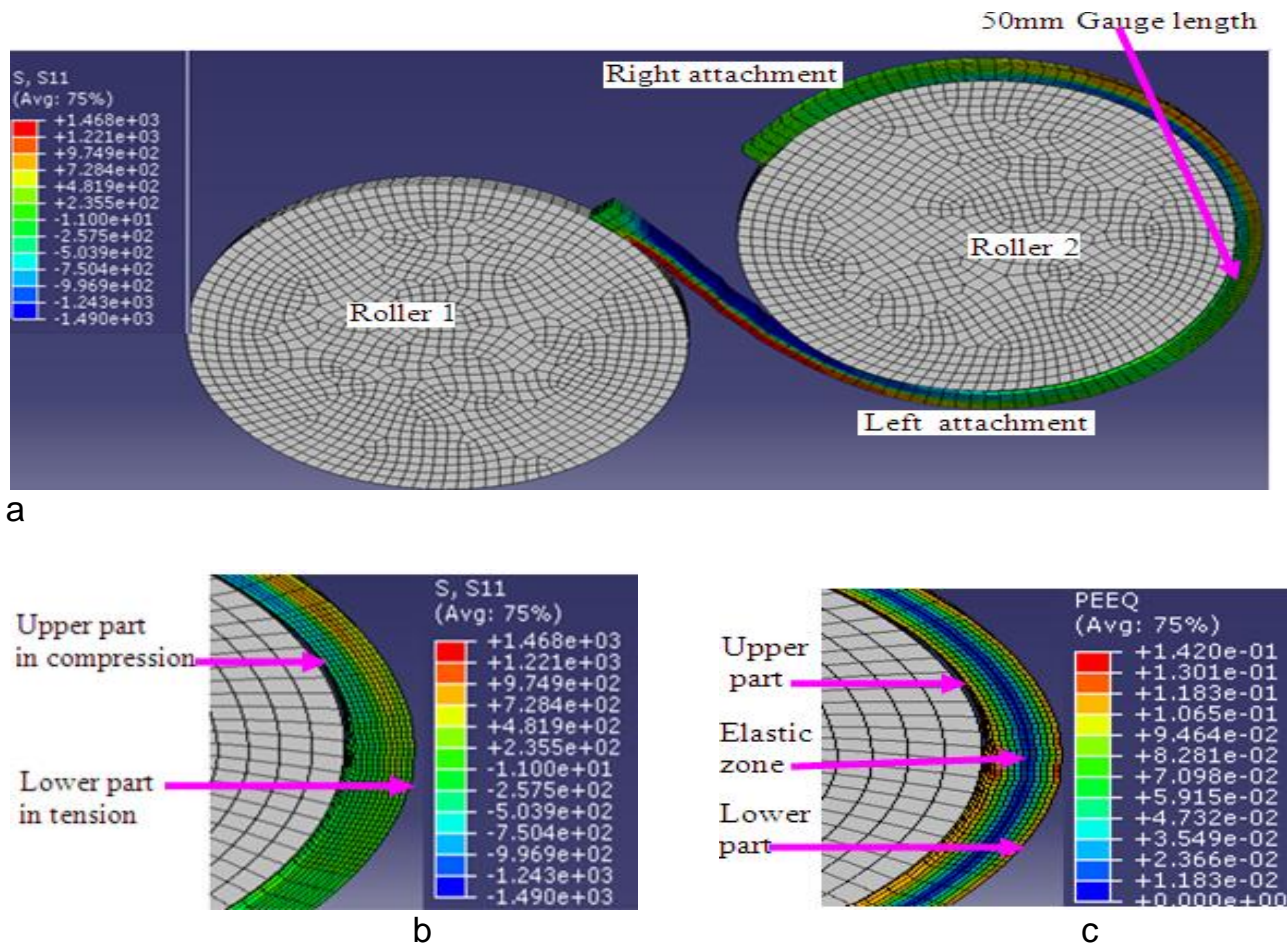


**Figure 7.** Deformed shape showing longitudinal axial stress (MPa) and equivalent plastic strain distributions in wire after reverse bending process simulation. a, Deformed shape and longitudinal axial stress distribution in whole wire length; b, longitudinal axial stress distribution; c, equivalent plastic strain distribution.

stresses in the  $S_{11}$  contour plot represent tensile axial stresses, while negative axial stresses represent compressive axial stresses. The highest tensile stress is indicated at the top of the contour plot with the deepest red colour while the highest compressive stress is indicated at the bottom of the contour plot with the deepest blue colour. The through thickness equivalent plastic strain (designated as PEEQ in the contour plot) distribution in the tensile test specimen after the bending, reverse bending and straightening process simulations are shown in Figures 5c, 7c and 8c, respectively.

### Tensile testing simulation results

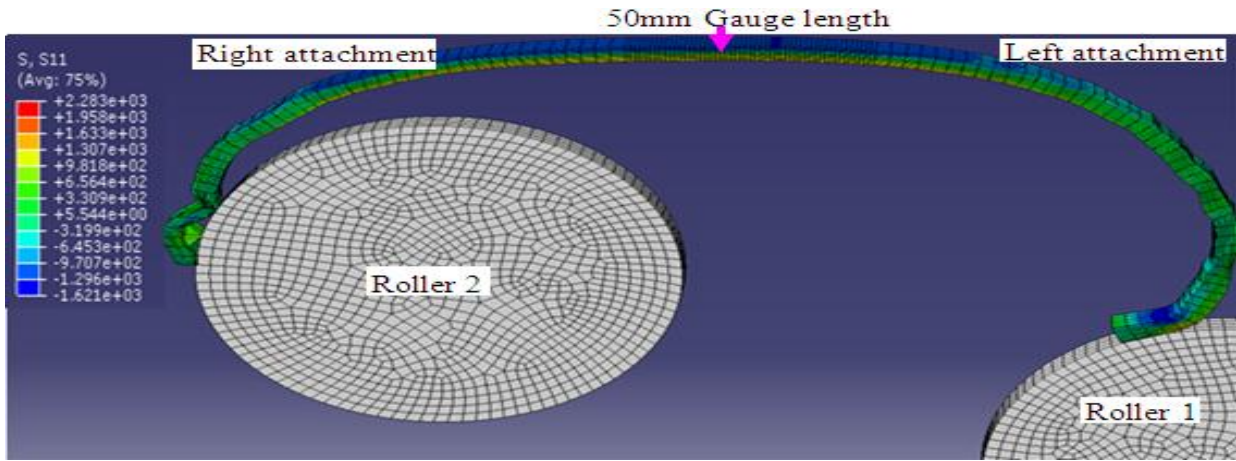
The fracture shapes predicted by the simulations conducted with the unbent wire specimen within the rollers-attachments-specimen assembly and with the unbent wire specimen alone are shown in Figures 9 and 10, respectively. The deformed shape of the entire 305 mm long wire showing the longitudinal axial stress distribution in the wire and the fractured RBS tensile test

specimen within the rollers-attachments-specimen assembly after the tensile testing simulation is shown in Figure 11. The fractured shape of the numerically simulated RBS specimen subjected to tensile testing simulation is shown in Figure 12a and the fractured experimentally RBS tensile specimen subjected to laboratory tensile testing is shown in Figure 12b.

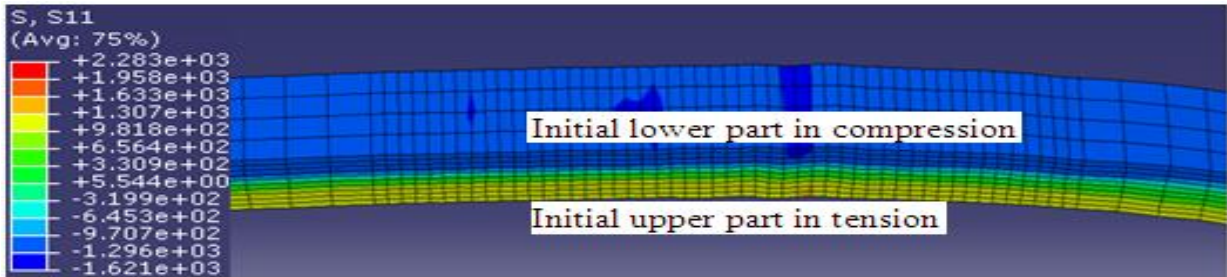
The normalized force-displacement curves obtained from the simulations of the tensile testing of the unbent wire specimen alone and the unbent wire specimen within the rollers-attachments-specimen assembly are shown in Figure 13. The normalised force-displacement curves obtained from the simulation of the tensile testing of the numerically simulated RBS specimen and the laboratory tensile testing of the experimentally RBS tensile specimen are shown in Figure 14.

### DISCUSSION

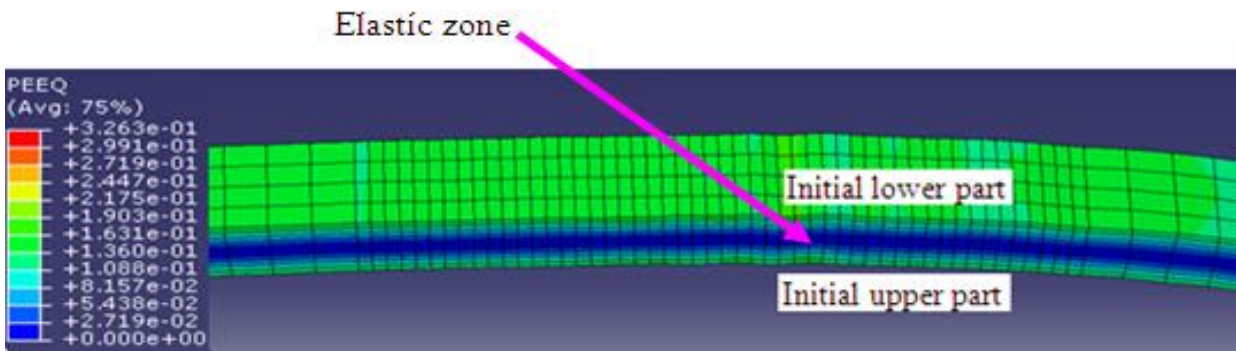
As shown in Figure 5b, after the bending simulation, the upper and the lower parts of the wire specimen are



a



b



c

**Figure 8.** Deformed shape showing longitudinal axial stress (MPa) and equivalent plastic strain distributions in wire after straightening process simulation. a, Deformed shape and stress distribution in whole wire length; b, longitudinal axial (MPa) stress distribution; c, equivalent plastic strain distribution.

subjected to tensile and compressive axial stresses, respectively, which agrees with the stress pattern in a bent wires stated by Gillstrom and Jarl (2006). The tensile and compressive axial stresses caused plastic deformations of the upper and the lower parts of the wire specimen as shown by the equivalent plastic strains in the specimen in Figure 5c. The middle 20% (approximately two element layers) of the wire specimen's thickness, where the neutral axis lies remains

elastic with zero equivalent plastic strain as shown in Figure 5c. The peak stress and strain occurred at the surfaces of the wire specimen, which agrees with what is reported by Tvergaard (1987) and further shows the accuracy of the bending simulation. The peak stress and strain occurred at the surfaces of the wire because the elements at the surfaces of the wire experienced the highest stress and strain.

Calculating the maximum strain in the wire with a

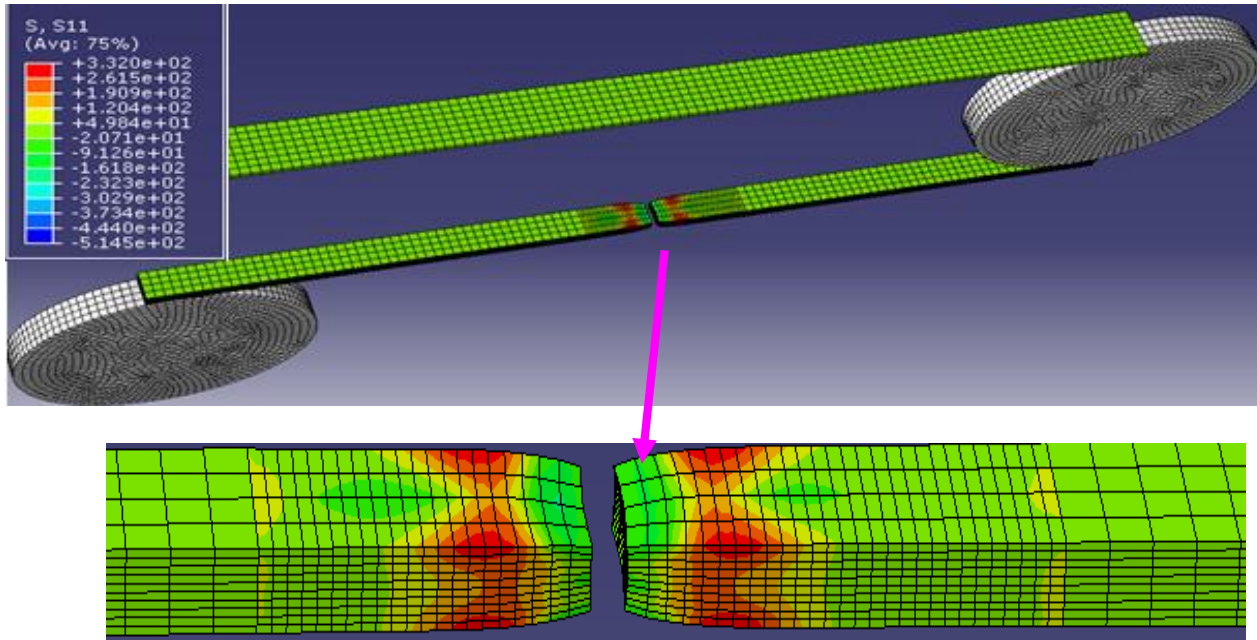


**Figure 9.** Fractured unbent specimen from simulation conducted with wire specimen within the rollers-attachments-specimen assembly.

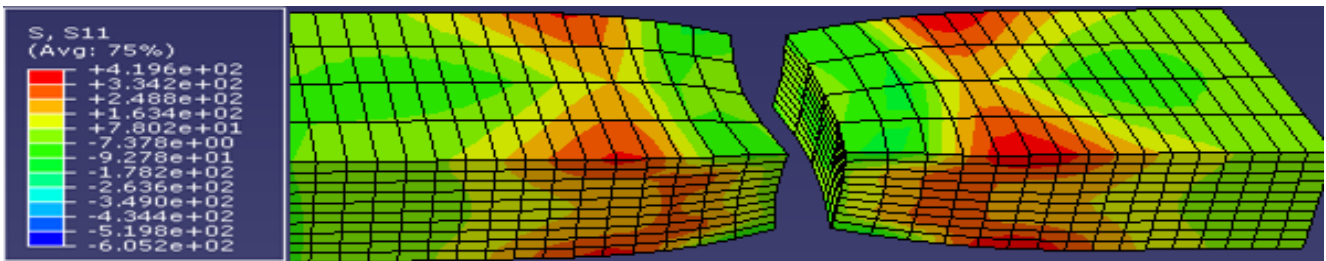


**Figure 10.** Fractured unbent specimen from simulation conducted with wire specimen alone.

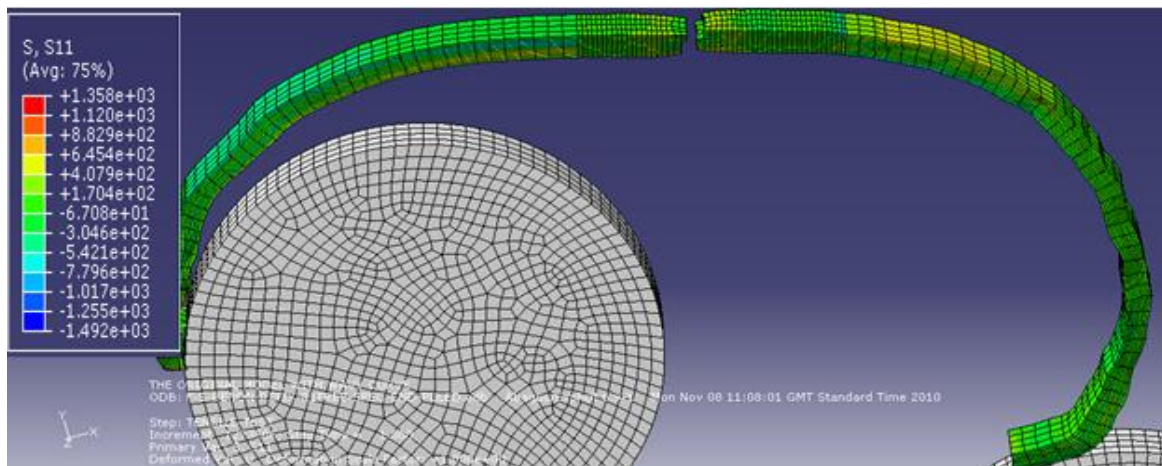
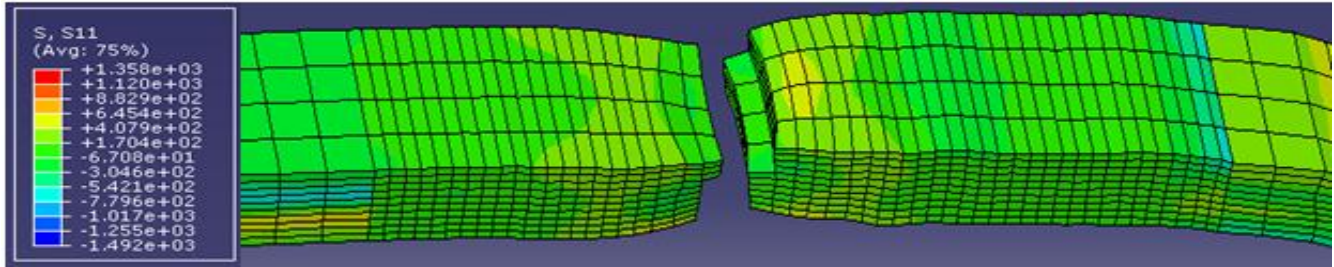


**Figure 11.** Deformed shape of the whole wire length showing the longitudinal axial stress (MPa) distribution in the wire and the fractured RBS specimen.



a



b

Figure 12. Fractured numerically and experimentally RBS specimens after tensile testing. a, Fractured numerically RBS specimen; b, fractured experimentally RBS specimen.

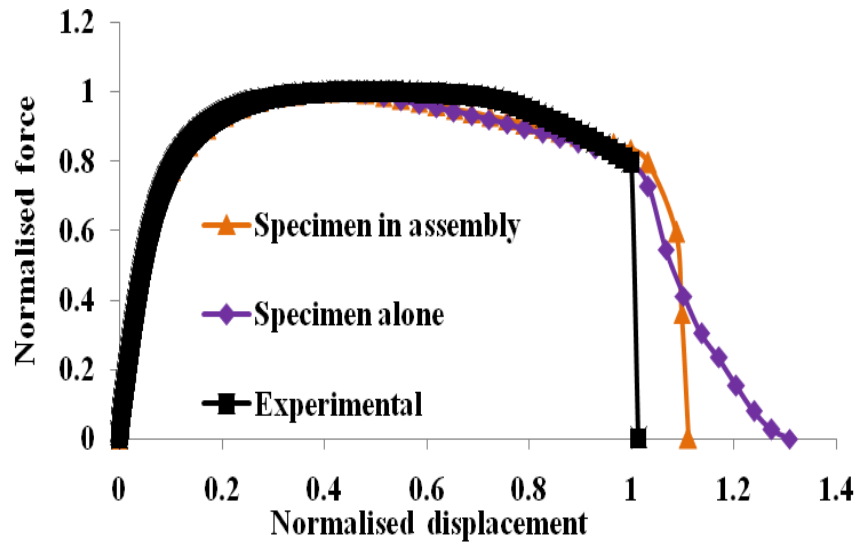


Figure 13. FE force-displacement curves from tensile testing of unbent wire specimen alone and wire specimen within rollers-attachments-specimen assembly.

thickness ( $T$ ) of 5 mm, bent over a roller of diameter ( $D_r$ ) of 100 mm with the expression given in Equation 1 as shown in Equation 7 gives a maximum strain of 0.048. The maximum strain of 0.043 predicted by the bending simulation as shown in the equivalent strain contour plot in Figure 5c agrees well with the maximum strain value of 0.048 calculated with the analytical expression. This further demonstrates the accuracy of the bending

simulation.

$$e = \frac{T}{T + D_r} = \frac{5}{5 + 100} = 0.048 \tag{7}$$

As shown in Figures 6, 7a and 7b, the initial upper part of the wire is now subjected to compressive stress and the initial lower half is now subjected to tensile stress during

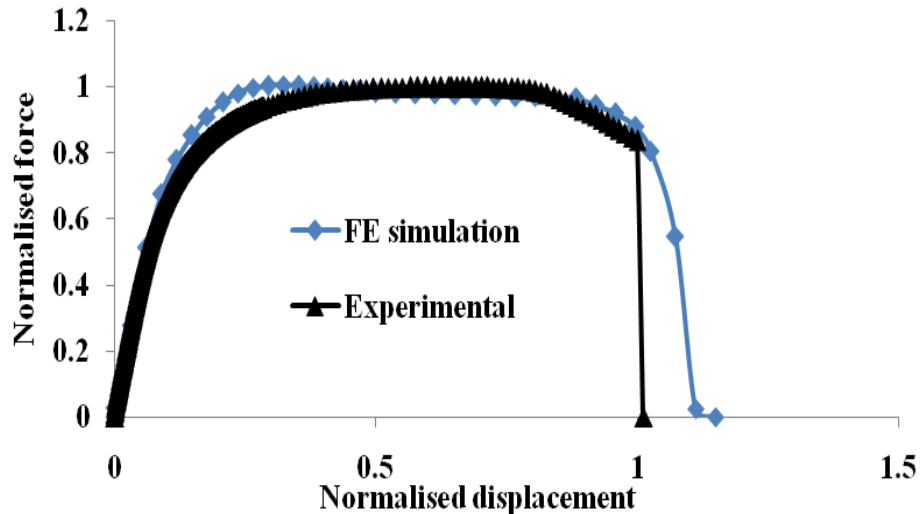


**Figure 14.** Experimental and FE force-displacement curves from tensile testing of RBS wire specimen.

and after the reverse bending simulation as a result of strain/stress reversal associated with the reverse bending operation. The true thickness deformation pattern of the wire specimen after the reverse bending simulation is similar to that predicted by the bending simulation as the upper and the lower parts of the wire specimen were plastically deformed, while the middle 20% of the wire specimen thickness, within which the neutral axis lies remains elastic with zero equivalent plastic strain as shown in Figure 7c.

The initial upper part and the initial lower part of the wire specimen at the beginning of the simulation is now the lower part and the upper part of the wire specimen that has undergone bending, RBS and are in tension and compression respectively as shown in Figures 8b and c. From Figure 8c, approximately the middle 20% of the wire specimen thickness also remains elastic after the straightening simulation, while the remaining outer portions of the wire specimen have been plastically deformed. The stress and the strain in the RBS specimen at the end of the straightening simulation represent the residual stress and the accumulated plastic strain in the tensile test specimen at the beginning of the tensile testing simulation. Thus, the upper and lower parts of the RBS wire specimen that was subjected to tensile testing simulation had undergone cyclic tensile and compressive plastic deformations, with residual compressive and tensile stresses respectively, while the middle 20% of the thickness of the wire remained elastic. This leaves the RBS wire specimen with an unbalanced residual stress distribution and a non-uniform through thickness deformation.

The fracture shapes shown in Figures 9 and 10, and the force-displacement curves shown in Figures 13 predicted by the simulations conducted with the unbent

wire specimen in the rollers-attachments-specimen assembly and the unbent wire specimen alone are in a good agreement. This indicates that the boundary conditions applied to the reels, attachments and specimen during the tensile testing simulation are appropriate as they have negligible impact on the fracture shape and the tensile response of the specimen with a maximum of 0.19% difference between the tensile properties (occurring in the displacement at fracture) predicted by the two simulations. The good agreements in the fracture shapes shown in Figure 12 and in the force-displacement curves shown in Figure 14 predicted by the simulation of the tensile testing of the numerically simulated RBS wire specimen and the curves from the laboratory tensile testing of the experimentally RBS wire specimen shows the accuracy of the bending, reverse bending, straightening and tensile testing simulations.

## CONCLUSION

In this paper, the details of the simulation procedures employed for the simulation of the bending and reverse bending of a flat carbon wire as it is conducted in practice, and the straightening and tensile testing simulation processes were presented. It was demonstrated that the bending simulation procedure employed was able to predict a maximum bending strain that agrees with an existing analytical expression. It was also demonstrated that the bending, reverse bending, straightening and tensile testing simulation procedures employed were appropriate to predict the bending and tensile responses of a flat wire subjected to reverse bending, straightening and tensile testing. This is evidenced in the good agreement in the fracture shapes and the tensile

responses of the experimentally and numerically RBS wire tensile specimens. This paper thus presents a numerical tool to be used as a virtual experiment in the investigation of the effect of the combination of reverse bending and defects on the tensile properties of wires.

## REFERENCES

- Adewole KK, Race JM, Bull SJ (2011). Determination of the appropriate fracture mechanism for tensile armour wires using micromechanical model-based fracture mechanics. Proc AES-ATEMA 2011, Montreal, Canada, August 1-5 (2011).
- Burks B, Middleton J, Armentrout D, Kumosa M (2010). Effect of excessive bending on residual tensile strength of hybrid composite rods. *Compos. Sci. Technol.*, 70: 1490-1496.
- Burks BM, Armentrout DL, Baldwin M, Buckley J, Kumosa M (2009). Hybrid composite rods subjected to excessive bending loads. *Compos. Sci. Technol.*, 69(15-16): 2625-2632.
- Carbonnie J, Thuillier S, Sabourin F, Brunet M, Manach PY (2008). Comparison of the work hardening of metallic sheets in bending–unbending and simple shear. *Inter. J. Mech. Sci.*, 51: 122-130.
- Escoe KA (2006). Piping and pipeline assessment guide, Gulf Professional Publishing. ISBN 13: 978-0-7506-7880-3.
- Firat M (2007). U-channel forming analysis with an emphasis on springback deformation. *Mater. Des.*, 28: 147-154.
- Gau JT, Kinzel GL (2001). A new model for springback prediction in which the Bauschinger effect is considered. *Inter. J. Mech. Sci.*, 43(8): 1813-1832.
- Gillstrom P, Jarl M (2006). Mechanical descaling of wire rod using reverse bending and brushing, *J. Mater. Process. Technol.*, 172(3): 332-334.
- Ken-ichiro M (2001). Simulation of materials processing: theory, methods and applications: proceedings of the 7th International Conference on Numerical Methods in Industrial Forming Processes--NUMIFORM 2001, pp. 711-721. Paper presented by Cedric Xia, Z.
- Moir S, Preston J (2002). Surface defects- evolution and behaviour from cast slab to coated strip. *J. Mater. Process. Technol.*, 125-126: 720-724.
- Peet S, Wilde A (2001). Laminations-origin, detection and assessment. Congreso Internacional de Ductos, Merida Yucatan, 14-16 November, 2001.
- Simulia (2007). Abaqus documentation, Abaqus Incorporated, Dassault Systemes.
- Smith BO, Jenning APH, Grimshaw AG (1957). A portable lamination detector for steel sheet, The British Iron and Steel Research Association, Battersea Park Road, London.
- Tvergaard V (1987). Ductile shear failure at the surface of a bent specimen. *Mech. Mater.*, 6: 53-69.
- United States Bureau of Reclamation (1994). Prestressed Concrete Pipe Failure Jordan Aqueduct, Reach 3". All U.S. Government Documents (Utah Regional Depository), Paper 284. <http://digitalcommons.usu.edu/govdocs/284>, assessed on 20/01/2012.